Acta Crystallographica Section D
Biological Crystallography
ISSN 0907-4449

Atomic resolution structure of pseudoazurin from the methylotrophic denitrifying bacterium *Hyphomicrobium denitrificans*: structural insights into its spectroscopic properties

Daisuke Hira, Masaki Nojiri* and Shinnichiro Suzuki

Bioinorganic Chemistry Laboratory, Department of Chemistry, Graduate School of Science, Osaka University, 1-1 Machikaneyama, Toyonaka, Osaka 560-0043, Japan

Correspondence e-mail: nojiri@ch.wani.osaka-u.ac.jp

Received 7 October 2008
Accepted 29 November 2008

PDB Reference: pseudoazurin, 3ef4, r3ef4sf.

The crystal structure of native pseudoazurin (HdPAz) from the methylotrophic denitrifying bacterium *Hyphomicrobium denitrificans* has been determined at a resolution of 1.18 Å. After refinement with *SHELX* employing anisotropic displacement parameters and riding H atoms, R_{work} and R_{free} were 0.135 and 0.169, respectively. Visualization of the anisotropic displacement parameters as thermal ellipsoids provided insight into the atomic motion within the perturbed type 1 Cu site. The asymmetric unit includes three HdPAz molecules which are tightly packed by head-to-head cupredoxin dimer formation. The shape of the Cu-atom ellipsoid implies significant vibrational motion diagonal to the equatorial *xy* plane defined by the three ligands (two His and one Cys). The geometric parameters of the type 1 Cu site in the HdPAz structure differ unambiguously from those of other pseudoazurins. It is demonstrated that their structural aspects are consistent with the unique visible absorption spectrum.

1. Introduction

The geometric and electronic structures of active sites in metalloproteins play a central role in the biological function of these proteins. The family of blue copper proteins show large variations in both active-site geometry and redox properties depending upon the actual ligands bound to the Cu centre and have been the subject of many theoretical and experimental studies (Solomon *et al.*, 2004; Gray *et al.*, 2000). These have revealed the importance of both metal–ligand coordination and the protein environment in tuning the redox properties of the metal centre.

Pseudoazurin (PAz) is a soluble periplasmic redox protein containing approximately 120 residues that is found in denitrifying bacteria and methylotrophs. The protein was first isolated from *Achromobacter cycloclastes* IAM1013 by Iwasaki & Matsubara (1973) and was subsequently named pseudoazurin by Ambler & Tobari (1985). PAz is produced in methylotrophs under conditions of high copper concentration when the cells are grown in methanol (Liu *et al.*, 1986). In denitrifying bacteria, PAz donates an electron to nitrite reductase (NIR) under anaerobic conditions (Moir *et al.*, 1993; Kukimoto *et al.*, 1996; Suzuki *et al.*, 1999).

PAz is a typical blue copper protein, possessing a single Cu atom at the active site. It provides an intense absorption band owing to the ligand cysteine S atom $S\rightarrow Cu^{II}$ charge-transfer transition near 600 nm ($\varepsilon = \sim 3700\ M^{-1}\ cm^{-1}$) and two clear absorption maxima near 450 and 750 nm; the ~600 nm band is the most intense ($\varepsilon_{\sim 450}/\varepsilon_{\sim 600} = 0.4$–$0.5$; Kohzuma *et al.*, 1995). X-ray crystallographic analysis of PAz has demonstrated that

the protein consists of eight β-strands forming a β-barrel and two helices at the C-terminus. The Cu atom is coordinated by two histidines, one cysteine and one methionine with a distorted tetrahedral geometry (Petratos *et al.*, 1987; Williams *et al.*, 1995; Inoue *et al.*, 1999).

Recently, we have reported that a methylotrophic denitrifying bacterium, *Hyphomicrobium denitrificans*, also produces a pseudoazurin (HdPAz) when the cells are grown anaerobically in a methanol-containing medium with a high concentration of copper (Hira *et al.*, 2007). Although HdPAz exhibits high amino-acid sequence similarity (40–60%) to well known pseudozurins, it displays a unique spectroscopic property by exhibiting a larger absorption coefficient ratio at 445 and 585 nm ($\varepsilon_{\sim450}/\varepsilon_{\sim600}$ = 0.86). Furthermore, it has been demonstrated that HdPAz functions as an electron mediator between methanol oxidation initiated by the methanol dehydrogenase–cytochrome c_L system (Nojiri *et al.*, 2006) and nitrite reduction by NIR (Nojiri *et al.*, 2007) in the periplasm of *H. denitrificans*.

Here, we describe the crystal structure of native HdPAz at a resolution of 1.18 Å. The substantially higher resolution permits significant refinement of the perturbed type 1 Cu-site structure in the HdPAz molecule. Moreover, the quality of the crystallographic data allows refinement of the anisotropic displacement parameters (ADPs); visualization of the ADPs as thermal ellipsoids facilitates an evaluation of the atomic motions in the Cu coordination sphere.

2. Material and methods

2.1. Purification of native HdPAz

Purification of the oxidized form of HdPAz was carried out as described previously (Hira *et al.*, 2007). The concentration was determined from the absorbance of oxidized HdPAz at 585 nm (ε = 2200 M^{-1} cm^{-1}) and pH 6.0.

2.2. Crystallization, data collection and structure refinement

HdPAz crystals were obtained by the hanging-drop vapour-diffusion method. The protein was concentrated to ~3.0 m*M* in 10 m*M* potassium phosphate buffer pH 6.0 and mixed with an equal volume of reservoir solution consisting of 3.2 *M* ammonium phosphate and 50 m*M* potassium phosphate pH 4.0. Greenish-blue crystals separated out after 2 d at 277 K. For data collection at 100 K, the crystals were flash-frozen in a cryocooled nitrogen-gas stream after being briefly dipped into a reservoir solution supplemented with 20%(*w*/*v*) glycerol.

Diffraction data sets were collected from the HdPAz crystal on beamline 44XU of SPring-8 (Japan Synchrotron Radiation Research Institute, Hyogo, Japan) using a radiation wavelength of 0.9 Å and a Bruker DIP-6040 detector system. To cover the entire range of intensities, the data were collected in two sweeps with differing crystal-to-detector distances (200 and 450 mm, with corresponding highest possible resolutions of 1.1 and 2.0 Å) and an exposure time of 5 s for both high- and low-resolution images. The X-ray beam size was 0.05 × 0.05 mm, which was smaller than the crystal size (0.5 × 0.4 × 0.3 mm). After the first data collection, the crystal was translated by 0.05 mm along the spindle axis. The number of frames was 180 (the oscillation range was 1°) per data set and the total exposure time was 900 s per data set. The absorbed X-ray dose after collection for each data set, calculated using the program *RADDOSE* (Murray *et al.*, 2004), was ~0.12×10^7 Gy, which is approximately one thirtieth of the experimentally determined Garman limit of 3×10^7 Gy. The data were processed with the *HKL* program suite (Otwinowski & Minor, 1997). The highest resolution of 1.18 Å was chosen on the basis of the criteria that more than 80% of reflections in the highest shell satisfied $I/\sigma(I) > 2$ and the average $I/\sigma(I)$ was greater than 2.0 for all reflections in the shell. The isotropic crystal mosaicity parameter refined to 0.29°.

The crystal belonged to space group *C*2, with three HdPAz molecules per asymmetric unit. The crystal structure was determined by molecular replacement using the program *MOLREP* (Vagin & Teplyakov, 1997) from the *CCP*4 suite (Collaborative Computational Project, Number 4, 1994). The structure of PAz from *Paracoccus pantotrophus* (PDB code 1adw; Williams *et al.*, 1995) was used as the search model after first omitting Cu, waters and the side chains of amino-acid residues which differed between the two proteins. One cycle of rigid-body refinement and minimization at 44.9–3.0 Å resolution was performed with *CNS* (Brünger *et al.*, 1998). The resulting initial model gave an R_{work} and R_{free} of 36% and 40%, respectively. Noncrystallographic symmetry (NCS) restraints were employed during the early refinement of the HdPAz model at 1.5 Å resolution and the model was then manually rebuilt and adjusted using *XtalView* (McRee, 1999). On the basis of this model, an electron-density map was used to fit the omitted side chains in order to generate the starting model for refinement. Without NCS, several further cycles of geometry-restrained positional refinement and isotropic *B*-factor refinement using the program *REFMAC* (Murshudov *et al.*, 1997) from the *CCP*4 suite resulted in an R_{work} of 24% (120 961 reflections with $|F_o| > 0$) and an R_{free} of 25% (for 6431 reflections), during which the resolution was extended to its highest limit. This model was further refined using *SHELX*97 (Sheldrick, 2008). After 20 cycles of conjugate-gradient least-squares refinement with isotropic thermal parameters, the model was thoroughly examined for possible errors using $2m|F_o| - D|F_c|$ (1.5σ) and $|F_o| - |F_c|$ (±3.0σ) difference maps. Water molecules were added to the model using the automated water-searching program *SHELXWAT* and were then further refined. Progress was made with conjugate-gradient anisotropic refinement using six-parameter anisotropic displacement parameters with bond-length, bond-angle, planarity, chirality and antibumping restraints. The copper-coordination geometry was not restrained. There was a dramatic improvement in R_{work} and R_{free} to 14.7% and 18.0%, respectively. In addition, 14 residues were modelled in multiple conformations. The occupancies of the atoms modelled in two alternative conformations were fixed at 0.5. The final values of R_{work} and R_{free} for the model with implemented riding H atoms were 12.2% and 15.6%, respectively, for 100 866 reflections with $|F_o| > 4\sigma(F_o)$ and were 13.5% and

Table 1
Crystallographic data-collection and refinement statistics.

Values in parentheses are for the highest resolution shell.

Data statistics	
Wavelength (Å)	0.9
Resolution (Å)	44.9–1.18 (1.22–1.18)
Space group	*C*2
Unit-cell parameters	
a (Å)	97.69
b (Å)	50.62
c (Å)	82.38
β (°)	90.98
Unit-cell volume (Å^3)	4073263
Solvent content (%)	50
Mosaicity (°)	0.29
No. of measured reflections	814168
No. of independent reflections	127401
No. of frames per data set	180
Total X-ray exposure per data set (s)	900
Completeness (%)	95.8 (85.2)
Redundancy	3.8 (2.9)
R_{merge} (%)	4.1 (49.0)
$\langle I\rangle/\langle\sigma(I)\rangle$	43.6 (2.8)
Refinement statistics	
R_{work} (%)	13.5
R_{free}† (%)	16.9
No. of non-H atoms	
No. of protein, phosphate, Cu atoms	3010
No. of solvent atoms	500
R.m.s. deviation from ideal values	
Bond length (Å)	0.014
Angle distance (Å)	0.033
Average B_{iso} (Å^2)	
Protein	16.8
Cu	11.4
Phosphate	30.8
Solvent	34.6
Average anisotropy for all protein atoms	0.48
Ratio of data to anisotropic parameters	5.7
Ramachandran plot‡, residues in	
Most favoured regions (%)	91.3
Additional and generously allowed regions (%)	8.7

† 5% random test set (6376 reflections). ‡ Calculated using *PROCHECK*.

16.9%, respectively, for all 121 025 reflections in the working data set. The final model was checked for stereochemical quality using *PROCHECK* (Laskowski *et al.*, 1993) and *MOLPROBITY* (Lovell *et al.*, 2003). Data-collection and refinement statistics are summarized in Table 1.

3. Results and discussion

3.1. Quality of the structure and overall fold

The crystallographic asymmetric unit contains three HdPAz molecules, labelled *A*, *B* and *C*. With a few exceptions, the protein electron density was unambiguous throughout. The entire backbone could be modelled with full occupancy in all three molecules. Several surface side chains could not be completely modelled owing to weak density and were therefore truncated (Lys10*A* C$^\gamma$, C$^\delta$, C$^\varepsilon$ and N$^\zeta$, Lys39*A* C$^\varepsilon$ and N$^\zeta$, Lys58*A* N$^\zeta$, Lys71*A* N$^\zeta$, Lys106*A* C$^\gamma$, C$^\delta$, C$^\varepsilon$ and N$^\zeta$, Lys113*A* N$^\zeta$, Lys121*A* N$^\zeta$, Lys10*B* C$^\delta$, C$^\varepsilon$ and N$^\zeta$, Lys33*B* N$^\zeta$, Lys39*B* C$^\varepsilon$ and N$^\zeta$, Lys63*B* C$^\delta$, C$^\varepsilon$ and N$^\zeta$, Lys71*B* N$^\zeta$, Lys106*B* C$^\gamma$, C$^\delta$, C$^\varepsilon$ and N$^\zeta$, Lys112*B* C$^\varepsilon$ and N$^\zeta$, Lys113*B* C$^\varepsilon$ and N$^\zeta$, Lys121*B* N$^\zeta$, Lys10*C* C$^\delta$, C$^\varepsilon$ and N$^\zeta$, Lys58*C* C$^\varepsilon$ and N$^\zeta$, Lys63*C* C$^\varepsilon$ and N$^\zeta$, Lys95*C* C$^\delta$, C$^\varepsilon$ and N$^\zeta$, Lys106*C* C$^\gamma$, C$^\delta$, C$^\varepsilon$ and N$^\zeta$, Lys121*C* N$^\zeta$). Several statistical indicators attest to the quality of the structure. For example, 91.3% of the nonglycine residues occupy the favoured region of the Ramachandran plot and there are no residues in the disallowed regions. The root-mean-square deviations (r.m.s.d.s) of the bond lengths and angle distances from the ideal values are 0.014 and 0.033 Å, respectively.

As expected, the HdPAz molecule displays a characteristic *β*-barrel folding structure with two C-terminal *α*-helices (Fig. 1). The major fold is a *β*-sandwich consisting of two *β*-sheets stacked face-to-face: *β*-sheet I consists of *β*1 (residues 2–10), *β*2a (16–20), *β*3 (31–35) and *β*5 (65–68) and *β*-sheet II contains *β*2b (residues 23–26), *β*4 (43–45), *β*6 (73–78) and *β*7 (88–93). Interestingly, residue Lys58 in the random-coil region (residues 50–60) is defined as an isolated *β*-bridge by the Database of Secondary Structure of Proteins (DSSP; Kabsch & Sander, 1983), although Val57 O and Gly59 N directly hydrogen bond to Ser45 N and Ala43 O in the *β*4 strand, respectively. Therefore, the number of *β*-strands in HdPAz is seven, not eight as in other pseudoazurins (Petratos *et al.*, 1987; Williams *et al.*, 1995; Inoue *et al.*, 1999). A single *cis*-proline residue (Pro21), which is also conserved in other pseudoazurins, provides a twist separating the two *β*-sheets within the *β*-sandwich of HdPAz. The protein contains a type 1 Cu atom coordinated by His41, Cys79, His82 and Met87 ligands. Moreover, amino-acid sequence alignment of HdPAz with other pseudoazurins shows that HdPAz has one insertion at position 15 and one deletion at position 95 (Hira *et al.*,

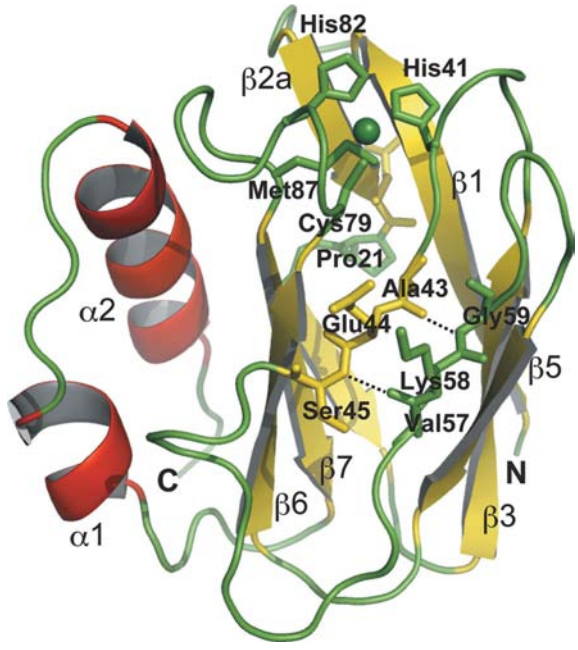

Figure 1
Ribbon drawing of one of the three HdPAz molecules in the asymmetric unit (*α*-helices, red; *β*-strands, yellow; loops, green). The Cu atom is shown as a green sphere. The side-chain atoms of the type 1 Cu ligands (His41, Cys79, His82 and Met87), *β*-strand 4 (Ala43, Glu44 and Ser45), the isolated *β*-bridge Lys58 and a single *cis*-proline residue (Pro21) are represented as sticks. The N- and C-termini are indicated by N and C, respectively. Several secondary structures are also labelled in the model. The dotted lines show hydrogen bonds.

2007): the insertion occurs in the first loop (residues 9–17) between β-strands β1 and β2a and the deletion in the loop (residues 94–98) between β-strand β7 and α-helix α1 in the HdPAz crystal structure.

The r.m.s.d.s for C^{α}-atom backbone positions between pairs of protein molecules in the asymmetric unit are $\leq$0.4 Å. The values between chains *A* and *B* and between chains *A* and *C* are 0.32 and 0.38 Å, respectively; these values are approximately twice that between chains *B* and *C* (0.17 Å). The r.m.s.d.s are believed to reflect conformational differences resulting from disparate crystal-packing environments. The largest area of difference is in the loop containing residues 105–108 of chain *A*. The O atom of Thr108*A* hydrogen bonds to the N atom of Lys112*A*, whereas the O atoms of Thr108*B* and Thr108*C* form hydrogen bonds to the N atoms of Ala111*B* and Ala111*C*, respectively (Fig. 2).

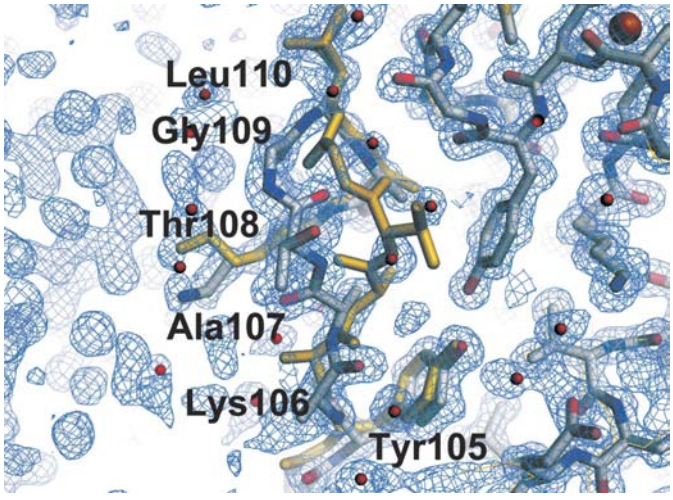

Figure 2
Conformational differences between the HdPAz molecules in the asymmetric unit. A close-up view is shown of the loop between residues 105 and 110 in chain *A*. Chain *C* (yellow) is superposed on chain *A* (grey). A σ_A-weighted $2F_{obs} - F_{calc}$ map contoured at 1.0σ is shown around the loop region.

One of the key features of HdPAz that distinguishes it from other pseudoazurins is the fact that HdPAz crystallizes to form a head-to-head cupredoxin dimer. Dimer formation occurs between chains *A* and *C* and between chain *B* and a crystallographically symmetric neighbouring chain *B* (*B*′; Fig. 3). The two dimers are almost identical and the Cu–Cu distances are 10.9 Å. The areas of the monomer surface that are solvent-inaccessible in the *AC* and *BB*′ dimers are ∼300 Å^2.

3.2. The perturbed type 1 Cu site

The Cu atom is located near the top surface, which has been called the 'northern surface' in the HdPAz molecule. In HdPAz, the Cu atom is coordinated to four ligands: His41 $N^{\delta1}$, His82 $N^{\delta1}$, Cys79 S^{γ} and Met87 S^{δ} (Fig. 4 and Table 2). The His41 ligand is located in the region between β3 and β4, while the other ligands are located in the loop region (the ligand-containing loop) between β6 and β7. Fig. 4(*a*) shows the electron density of the type 1 Cu site. The mean B_{iso} factors of the Cu ligands (with e.s.d.s in parentheses) are 11.38 (0.21), 10.32 (0.10), 10.74 (0.34) and 10.40 (0.14) Å^2 for His41 $N^{\delta1}$, Cys79 S^{γ}, His82 $N^{\delta1}$ and Met87 S^{δ}, respectively. The Cu atom has a mean B_{iso} factor of 11.43 (0.22) Å^2. These values and the high-quality electron density support the fact that the Cu site is extremely constrained compared with the protein moiety because of stabilization by the surrounding hydrogen-bond networks around the type 1 Cu site (Machczynski *et al.*, 2002; Yanagisawa *et al.*, 2006; Velarde *et al.*, 2007). The high-resolution data allowed the precise determination of not only the positions of the Cu and S atoms but also of the N atoms in the imidazole groups of the ligands.

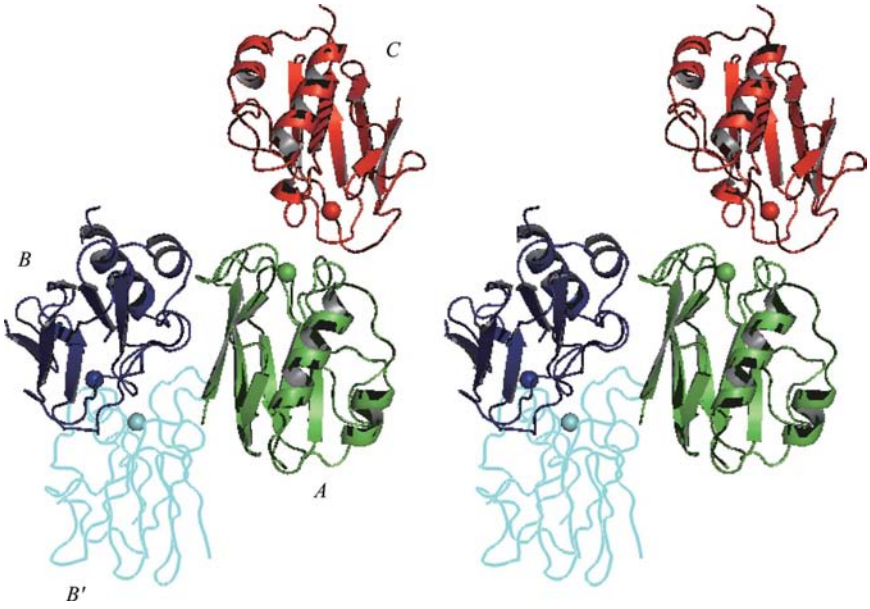

Figure 3
Stereoview of two head-to-head cupredoxin dimers in the HdPAz crystal. The three molecules in the asymmetric unit are depicted as ribbons (green, blue and red) and the neighbouring chain *B* (*B*′) is shown as a C^{α} trace (cyan). Each Cu atom is shown as a sphere.

The Cu site was further analysed in terms of its anisotropic nature. Thermal ellipsoids at the 50% probability level are shown in Fig. 4(*b*) for all the non-H atoms at the Cu site. Structures at atomic resolution are expected to have a mean anisotropy of ∼0.4–0.5 on a scale where an anisotropy of 1 corresponds to perfect isotropy and where extremely anisotropic atoms approach an anisotropy of 0. In HdPAz, the mean anisotropy of the structure was calculated to be 0.48 for the protein atoms and 0.56 for the Cu atoms. The mean calculated anisotropy of the amino acids for the copper ligands was 0.53. The thermal ellipsoid of the Cu atom exhibits an unambiguous elliptical shape which is diagonal to the equatorial *xy* plane defined by the three ligands His41 $N^{\delta1}$, Cys79 S^{γ} and His82 $N^{\delta1}$. Compared with the atomic resolution

Table 2
Comparison of the type 1 Cu site of HdPAz with those of four other proteins.

His_1 and His_2 are the first and second His ligands in the amino-acid sequence.

	PoPc†	AcPAz†	CBP†	AcNIR†	HdPAz‡
Distances (Å)					
$His_1\ N^{\delta1}-Cu$	1.91	1.95	1.93	2.04	2.00 (±0.005)
Cys $S^{\gamma}-Cu$	2.07	2.13	2.16	2.23	2.20 (±0.01)
$His_2\ N^{\delta1}-Cu$	2.06	1.92	1.95	2.03	2.03 (±0.015)
Met S^{δ}–Cu	2.82	2.71	2.61	2.49	2.55 (±0.035)
Angles (°)					
$His_1\ N^{\delta1}-Cu-Cys\ S^{\gamma}$	132	135	138	127	136 (±2)
$His_1\ N^{\delta1}-Cu-His_2\ N^{\delta1}$	97	100	99	101	96 (±0.5)
$His_1\ N^{\delta1}-Cu-Met\ S^{\delta}$	88	87	83	86	90 (±0.5)
Cys $S^{\gamma}-Cu-His_2\ N^{\delta1}$	121	115	110	108	109 (±0.5)
Cys $S^{\gamma}-Cu-Met\ S^{\delta}$	110	107	111	108	111 (±0.5)
$His_2\ N^{\delta1}-Cu-Met\ S^{\delta}$	101	107	112	127	114 (±1)
θ§	82	76	70	66	72 (±2)
φ¶	168	169	171	172	175 (±1.5)

† The structures of the Cu sites of poplar plastocyanin (PoPc), *A. cycloclastes* PAz (AcPAz), cucumber basic protein (CBP) and *A. cycloclastes* NIR (AcNIR) are taken from PDB entries 1plc, 1bqk, 2cbp and 2bw4, respectively. ‡ Averaged values of three Cu sites in the HdPAz molecules in the asymmetric unit; the errors are given in parentheses. § θ is the dihedral angle between the $His_1\ N^{\delta1}-Cu-His_2\ N^{\delta1}$ and Cys $S^{\gamma}-Cu-Met\ S^{\delta}$ planes. ¶ φ is the Cys $C^{\alpha}-C^{\beta}-S^{\gamma}-Cu$ torsion angle.

(1.13 Å) structure of azurin-II (Paraskevopoulos *et al.*, 2006), the Cu atom of HdPAz is more anisotropic than that of azurin-II (0.69); the thermal ellipsoid of the Cu atom of azurin-II is almost spherical. These differences are probably a consequence of the geometries of the type 1 Cu site in HdPAz and azurin-II; the type 1 Cu of azurin-II has an additional ligand (Gly45 O) in the axial position that HdPAz does not possess.

3.3. Structural insights into the spectroscopic properties of HdPAz

The visible absorption spectrum of HdPAz shows that the $\varepsilon_{\sim450}/\varepsilon_{\sim600}$ ratio (0.86) of HdPAz is larger than that (0.42) of the typical pseudoazurin *Achromobacter cycloclastes* PAz (AcPAz; Kohzuma *et al.*, 1995; Hira *et al.*, 2007); the colour of the former is more greenish-blue than that of the latter. This finding suggests that HdPAz has a more perturbed Cu site than AcPAz. Incidentally, the $\varepsilon_{\sim450}/\varepsilon_{\sim600}$ ratios of a classical blue copper protein, spinach plastocyanin (Katoh *et al.*, 1962), and the perturbed blue (green) copper proteins cucumber basic protein (CBP; Sakurai *et al.*, 1982) and the type 1 Cu of AcNIR (Suzuki *et al.*, 1997) are 0.12, 0.61 and 1.3, respectively.

Table 2 presents parameters of the type 1 Cu sites for five copper proteins. The Cu geometry of HdPAz is more like that of CBP (Guss *et al.*, 1996) than that of AcPAz. There has been much discussion about the origin of the spectral differences between classical (blue) and perturbed (green) Cu sites (Solomon *et al.*, 2004; LaCroix *et al.*, 1996, 1998; Lu *et al.*, 1993; Wijma *et al.*, 2003; Sato & Dennison, 2006). The spectral change from blue to green, which arises from the increasing absorption band near 450 nm, is associated with a tetragonal distortion of the ligand field of poplar plastocyanin (PoPc) in going to AcNIR (Table 2). Comparisons of the S—Cu bond distances of PoPc (Guss *et al.*, 1992) with those of AcNIR (Antonyuk *et al.*, 2005) show that the Met $S^{\delta}-Cu$ bond shortens by ∼0.3 Å and the Cys S^{γ}–Cu bond lengthens by ∼0.1 Å. Moreover, the Cys $S^{\gamma}-Cu-Met\ S^{\delta}$ plane rotates relative to the $His_1\ N^{\delta1}$–Cu–$His_2\ N^{\delta1}$ plane in a Jahn–Teller type distortion towards a more tetragonal geometry. The electronic/geometric correlation has been termed the 'coupled distortion', in which the stronger axial Met $S^{\delta}-Cu$ interaction produces a weaker Cys $S^{\gamma}-Cu$ bond and simultaneously results in a tetragonal Jahn–Teller distortion of the site (Solomon *et al.*, 2004; LaCroix *et al.*, 1996, 1998; Lu *et al.*, 1993; Wijma *et al.*, 2003). Therefore, we have focused on the dihedral angle (θ) between the S—Cu—S plane formed by the coordinating Cys79 and Met87 residues and the N—Cu—N plane formed by the coordinating His41 and His82 residues in HdPAz. Fig. 5 shows correlation plots between the absorption ratios ($\varepsilon_{\sim450}/\varepsilon_{\sim600}$) and the θ values (Fig. 5*a*) and between the θ values and the distance ratio of Met $S^{\delta}-Cu$ to Cys $S^{\gamma}-Cu$ (Fig. 5*b*). These graphs were produced by adding the recent high-resolution structural data of several blue Cu proteins to

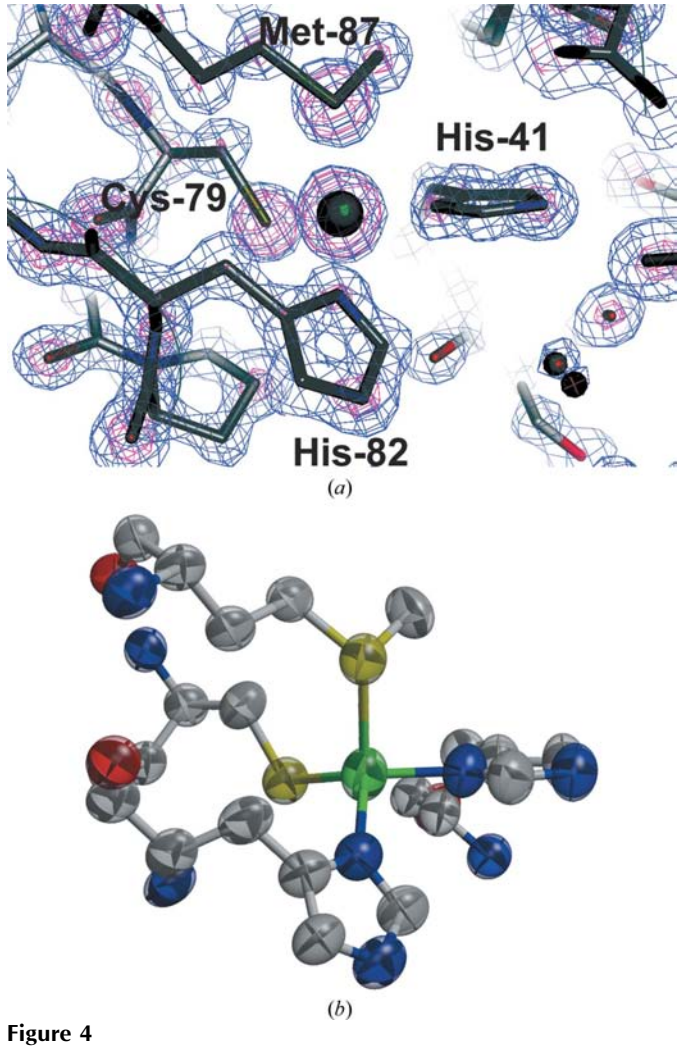

Figure 4
(*a*) $2F_{obs} - F_{calc}$ electron-density map contoured at 2.0σ (blue) and 5.0σ (red) of the perturbed type 1 Cu site in HdPAz. The Cu atom is shown as a green sphere. (*b*) Thermal ellipsoids at the 50% probability level for the Cu site viewed from the same direction as in (*a*). Ellipsoids are coloured according to their atom type. This figure was generated using *ORTEX* and *RASTER3D* (McArdle, 1994).

the correlation plot proposed by Wijma *et al.* (2003). Both theoretical and experimental arguments generally show that a high value of θ (close to 90°) correlates with a low value of the ratio of the two absorption peaks, $\varepsilon_{\sim450}$ (mainly Cys $S_\sigma \rightarrow$ Cu $3d_{x^2-y^2}$ charge-transfer transition)/$\varepsilon_{\sim600}$ (Cys $S_\pi \rightarrow$ Cu $3d_{x^2-y^2}$ charge-transfer transition; Pierloot *et al.*, 1998; Basunallick *et al.*, 2003). In the case of HdPAz, the slightly longer Cys79 S^γ—Cu and shorter Met87 S^δ—Cu distances relative to the corresponding distances of AcPAz and CBP may contribute to the electronic structure of the Cu site.

In order to identify the structural basis of the more perturbed geometry of the Cu site in HdPAz, the structure within 15 Å from the Cu atom of HdPAz was further investigated by comparison with those of other pseudoazurins. There is a relatively large difference at the position of Tyr83 compared with the corresponding residues of other pseudoazurins: the side chain of Tyr83 shifts to the protein interior to form a hydrogen bond to Tyr105, which is positioned in the loop containing residues 105–108 and is replaced by Ala or Val in the other proteins (Fig. 6). Thus, the loop containing residues 81–84 in HdPAz shifts slightly toward the C-terminal α-helices. The slight difference in this loop position brings about a displacement of the Cu atom (∼0.3 Å) which might lead to the longer Cys79 S^γ—Cu and shorter Met87 S^δ—Cu bonds compared with the corresponding bonds of AcPAz. Another difference is the slight rotation (∼7°) of the imidazole ring of ligand His41 in HdPAz. Indeed, the C^α chirality (angle) in Ser40 of HdPAz differs unambiguously from the corresponding residue Gly39 in AcPAz. Recently, it has been reported that the interaction between the His81 ligand and Met16 in AcPAz has the potential to affect the spectroscopic properties (Abdelhamid *et al.*, 2007; Yanagisawa *et al.*, 2008). In the well known structures of pseudoazurins, the Met16 (Met17 in HdPAz) residue interacts weakly with the imidazole of His81 (His82 in HdPAz) by forming a van der Waals contact (≤4.0 Å; Fig. 6). Spectroscopic and structure analyses of the Met16 mutants demonstrated that relaxation of the structural restraint to the imidazole leads to more perturbed Cu-site geometry (Abdelhamid *et al.*, 2007; Yanagisawa *et al.*, 2008).

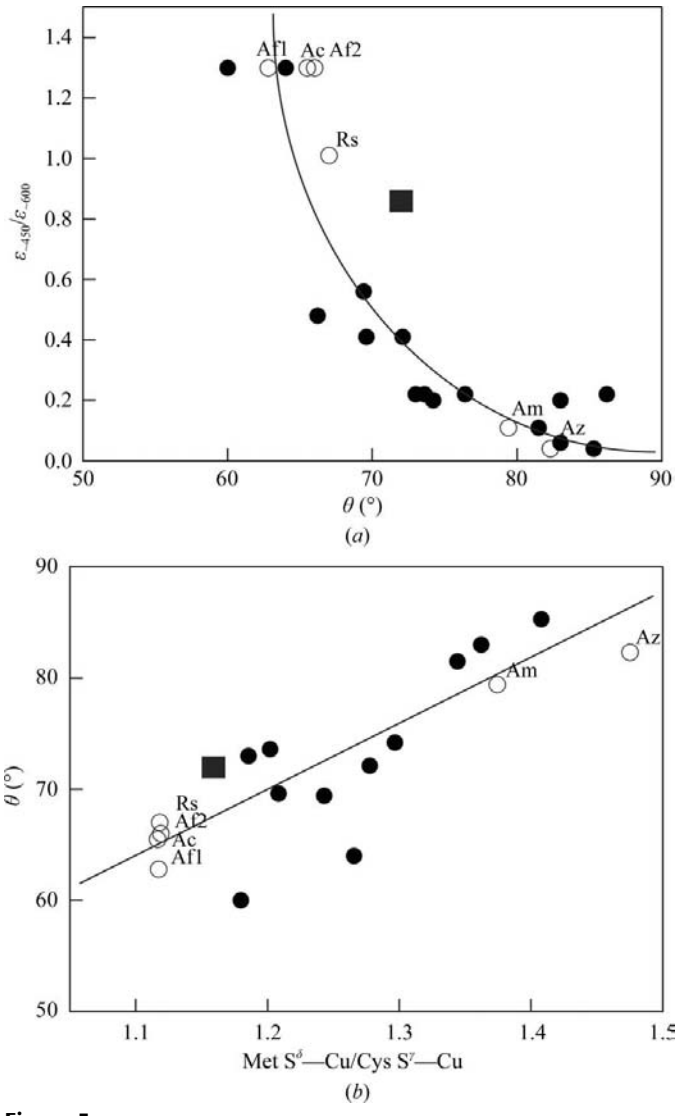

Figure 5
Relations between the ratio of the absorbance at near 450 and 600 nm *versus* dihedral angle θ values (*a*) and the θ values *versus* the ratio of the Met S^δ—Cu and Cys S^γ—Cu bond distances (*b*). Filled circles, data from the paper reported by Wijma *et al.* (2003). Circles, additional plots from recent structural data of the blue Cu proteins AcNIR (Ac; PDB code 2bw4, Antonyuk *et al.*, 2005), azurin-II (Az; PDB code 2ccw, Paraskevopoulos *et al.*, 2006), AfNIR (Af1 and Af2; PDB codes 1sjm and 1snr, Tocheva *et al.*, 2004), amicyanin (Am; PDB code 1aac, Cunane *et al.*, 1996) and RsNIR (Rs; PDB code 1zv2, Jacobson *et al.*, 2005). Filled squares, HdPAz.

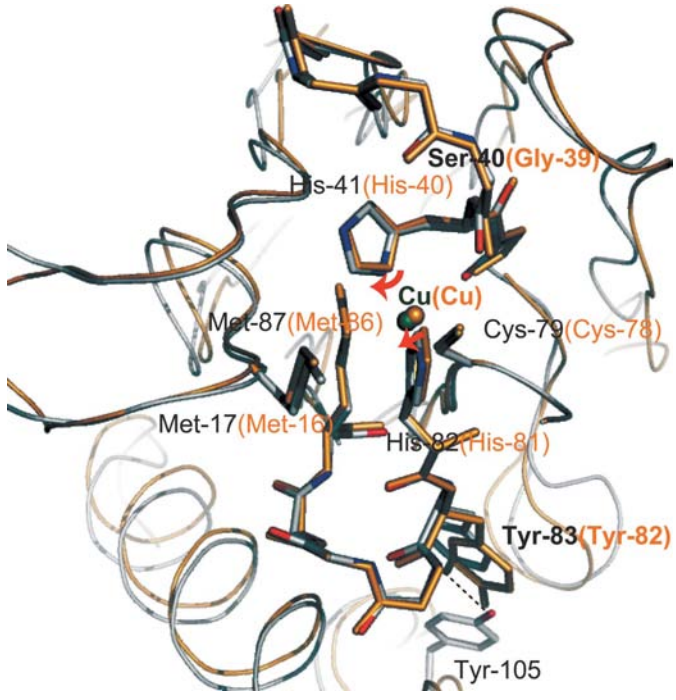

Figure 6
Superposition of the Cu site in HdPAz on that in AcPAz. Ligands and the residues that possibly affect the geometry of the Cu site are represented as grey (HdPAz) and orange (AcPAz) sticks. Each Cu atom is shown as green (HdPAz) and orange (AcPAz) spheres. The differences shown by red arrows indicate that the angle of the imidazole plane of His41 in HdPAz is rotated clockwise by ∼7° and that the imidazole group of His82 is slightly shifted to the left (∼0.3 Å).

These results may be consistent with several structural aspects observed in the atomic resolution structure of HdPAz.

4. Conclusion

In this study, the crystal structure of HdPAz has been solved at a resolution of 1.18 Å. This is the highest resolution structure of any pseudoazurin and the substantially higher resolution data permit significant refinement of the perturbed type 1 Cu site. Moreover, the visualization of anisotropic displacement parameters as thermal ellipsoids provides insights into the atomic motion within the perturbed type 1 Cu site. Three HdPAz molecules are contained in the asymmetric unit and are tightly packed by head-to-head cupredoxin dimer formation as in azurins. This is the first example of dimer formation in pseudoazurins. Although the overall structural features of the HdPAz monomer are similar to those of other pseudoazurins, the flattened tetrahedral geometry of the Cu site has significantly shorter Met S^{δ}—Cu and longer Cys S^{γ}—Cu bonds than the corresponding bonds in other pseudoazurins. These structural aspects at atomic resolution demonstrate that the unique spectroscopic properties of HdPAz are a consequence of extremely small differences in the geometry of the Cu site.

We thank Professor A. Nakagawa and Drs M. Suzuki, E. Yamashita and M. Yoshimura for their kind support in the collection of X-ray data. Synchrotron-radiation experiments were performed on beamline 44XU (Proposal No. 2006B6824 to MN) at SPring-8 with the approval of the Japan Synchrotron Radiation Research Institute. This work was supported in part by Grants-in-Aids for JSPS Fellows (to DH) from the Japan Society for Promotion of Science (JSPS), Encouragement of Young Scientists (B) 20750137 (to MN) and Scientific Research (B) 20350078 (to SS) from the Ministry of Education, Science, Sports and Culture of Japan and a Grant for Basic Science Research Projects from the Sumitomo Foundation (to MN).

References

Abdelhamid, R. F., Obara, Y., Uchida, Y., Kohzuma, T., Dooley, D. M., Brown, D. E. & Hori, H. (2007). *J. Biol. Inorg. Chem.* **12**, 165–173.
Ambler, R. P. & Tobari, J. (1985). *Biochem. J.* **232**, 451–457.
Antonyuk, S. V., Strange, R. W., Sawers, G., Eady, R. R. & Hasnain, S. S. (2005). *Proc. Natl Acad. Sci. USA*, **102**, 12041–12046.
Basunallick, L., Szilagyi, R. K., Zhao, Y., Shapleigh, J. P., Scholes, C. P. & Solomon, E. I. (2003). *J. Am. Chem. Soc.* **125**, 14784–14792.
Brünger, A. T., Adams, P. D., Clore, G. M., DeLano, W. L., Gros, P., Grosse-Kunstleve, R. W., Jiang, J.-S., Kuszewski, J., Nilges, M., Pannu, N. S., Read, R. J., Rice, L. M., Simonson, T. & Warren, G. L. (1998). *Acta Cryst.* D**54**, 905–921.
Collaborative Computational Project, Number 4 (1994). *Acta Cryst.* D**50**, 760–763.
Cunane, L. M., Chen, Z. W., Durley, R. C. & Mathews, F. S. (1996). *Acta Cryst.* D**52**, 676–686.
Gray, H. B., Malmström, B. G. & Williams, R. J. P. (2000). *J. Biol. Inorg. Chem.* **5**, 551–559.
Guss, J. M., Bartunik, H. D. & Freeman, H. C. (1992). *Acta Cryst.* B**48**, 790–811.
Guss, J. M., Merritt, E. A., Phizackerley, R. P. & Freeman, H. C. (1996). *J. Mol. Biol.* **262**, 686–705.
Hira, D., Nojiri, M., Yamaguchi, K. & Suzuki, S. (2007). *J. Biochem. (Tokyo)*, **142**, 335–341.
Inoue, T., Nishio, N., Suzuki, S., Kataoka, K., Kohzuma, T. & Kai, Y. (1999). *J. Biol. Chem.* **274**, 17845–17852.
Iwasaki, H. & Matsubara, T. (1973). *J. Biochem. (Tokyo)*, **73**, 659–661.
Jacobson, F., Guo, H., Olesen, K., Okvist, M., Neutze, R. & Sjolin, L. (2005). *Acta Cryst.* D**61**, 1190–1198.
Kabsch, W. & Sander, C. (1983). *Biopolymers*, **22**, 2577–2637.
Katoh, S., Shiratani, I. & Takamiya, S. (1962). *J. Biochem.* **51**, 32–40.
Kohzuma, T., Dennison, C., McFarlane, W., Nakashima, S., Kitagawa, T., Inoue, T., Kai, Y., Nishio, N., Shidara, S. & Suzuki, S. (1995). *J. Biol. Chem.* **270**, 25733–25738.
Kukimoto, M., Nishiyama, M., Tanokura, M., Adman, E. T. & Horinouchi, S. (1996). *J. Biol. Chem.* **271**, 13680–13683.
LaCroix, L. B., Shadle, S. E., Wang, Y., Averill, B. A., Hedman, B., Hodgson, K. O. & Solomon, E. I. (1996). *J. Am. Chem. Soc.* **118**, 7755–7768.
LaCroix, L. B., Shadle, S. E., Wang, Y., Averill, B. A., Hedman, B., Hodgson, K. O. & Solomon, E. I. (1998). *J. Am. Chem. Soc.* **120**, 9621–9631.
Laskowski, R. A., MacArthur, M. W., Moss, D. S. & Thornton, J. M. (1993). *J. Appl. Cryst.* **26**, 283–291.
Liu, M. Y., Liu, M. C., Payne, W. J. & LeGall, J. (1986). *J. Bacteriol.* **166**, 604–608.
Lovell, S. C., Davis, I. W., Arendall, W. B., de Bakker, P. I. W., Word, J. M., Prisant, M. G., Richardson, J. S. & Richardson, D. C. (2003). *Proteins*, **50**, 437–450.
Lu, Y., LaCroix, L. B., Lowery, M. D., Solomon, E. I., Bender, C. J., Peisach, J., Roe, J. A., Gralla, E. B. & Valentine, J. S. (1993). *J. Am. Chem. Soc.* **115**, 5907–5918.
Machczynski, M. C., Gray, H. B. & Richards, J. H. (2002). *J. Inorg. Biochem.* **88**, 375–380.
McArdle, P. (1994). *J. Appl. Cryst.* **27**, 438–439.
McRee, D. E. (1999). *J. Struct. Biol.* **125**, 156–165.
Moir, J. W., Baratta, D., Richardson, D. J. & Ferguson, S. J. (1993). *Eur. J. Biochem.* **212**, 377–385.
Murray, J. W., Garman, E. F. & Ravelli, R. B. G. (2004). *J. Appl. Cryst.* **37**, 513–522.
Murshudov, G. N., Vagin, A. A. & Dodson, E. J. (1997). *Acta Cryst.* D**53**, 240–255.
Nojiri, M., Hira, D., Yamaguchi, K., Okajima, T., Tanizawa, K. & Suzuki, S. (2006). *Biochemistry*, **45**, 3481–3492.
Nojiri, M., Xie, Y., Inoue, T., Yamamoto, T., Matsumura, H., Kataoka, K., Deligeer, Yamaguchi, K., Kai, Y. & Suzuki, S. (2007). *Proc. Natl Acad. Sci. USA*, **104**, 4315–4320.
Otwinowski, Z. & Minor, W. (1997). *Methods Enzymol.* **276**, 307–326.
Paraskevopoulos, K., Sundarajan, M., Surendran, R., Hough, M. A., Eady, R. R., Hillier, L. H. & Hasnain, S. S. (2006). *Dalton Trans.* **25**, 3067–3076.
Petratos, K., Banner, D. W., Beppu, T., Wilson, K. S. & Tsernoglou, D. (1987). *FEBS Lett.* **218**, 209–214.
Pierloot, K., De Kerpel, J. O. A., Ryde, U., Olsson, M. H. M. & Roos, B. O. (1998). *J. Am. Chem. Soc.* **120**, 13156–13166.
Sakurai, T., Okammoto, H., Kawahara, K. & Nakamura, A. (1982). *FEBS Lett.* **147**, 220–224.
Sato, K. & Dennison, C. (2006). *Chem. Eur. J.* **12**, 6647–6659.
Sheldrick, G. M. (2008). *Acta Cryst.* A**64**, 112–122.
Solomon, E. I., Szilagyi, R. K., George, S. D. & Basumallick, L. (2004). *Chem. Rev.* **104**, 419–458.
Suzuki, S., Deligeer, Yamaguchi, K., Kataoka, K., Kobayashi, K., Tagawa, S., Kohzuma, T., Shidara, S. & Iwasaki, H. (1997). *J. Biol. Chem.* **2**, 265–274.

Suzuki, S., Kataoka, K., Yamaguchi, K., Inoue, T. & Kai, Y. (1999). *Coord. Chem. Rev.* **190–192**, 245–265.
Tocheva, E. I., Rosell, F. I., Mauk, A. G. & Murphy, M. E. (2004). *Science*, **304**, 867–870.
Vagin, A. & Teplyakov, A. (1997). *J. Appl. Cryst.* **30**, 1022–1025.
Velarde, M., Huber, R., Yanagisawa, S., Dennison, C. & Messerschmidt, A. (2007). *Biochemistry*, **46**, 9981–9991.
Wijma, H. J., Boulanger, M. J., Molon, A., Fittipaldi, M., Huber, M., Murphy, M. E., Verbeet, M. P. & Canters, G. W. (2003). *Biochemistry*, **42**, 4075–4083.
Williams, P. A., Fülöp, V., Leung, Y. C., Chan, C., Moir, J. W., Howlett, G. D., Ferguson, S. J., Radford, S. E. & Hajdu, J. (1995). *Nature Struct. Biol.* **2**, 975–982.
Yanagisawa, S., Banfield, M. J. & Dennison, C. (2006). *Biochemistry*, **45**, 8812–8822.
Yanagisawa, S., Crowley, P. B., Firbank, S. J., Lawler, A. T., Hunter, D. M., McFarlane, W., Li, C., Kohzuma, T., Banfield, M. J. & Dennison, C. (2008). *J. Am. Chem. Soc.* **130**, 15420–15428.